Cell, Vol. 120, 209–221, January 28, 2005, Copyright ©2005 by Elsevier Inc. DOI 10.1016/j.cell.2004.11.054

The Haploinsufficient Tumor Suppressor p18 Upregulates p53 via Interactions with ATM/ATR

**Bum-Joon Park,[1] Jin Wook Kang,[1]
Sang Won Lee,[1] So-Jung Choi,[1]
Young Kee Shin,[1] Young Ha Ahn,[1]
Yun Hee Choi,[1] Dongho Choi,[2]
Kwang Soo Lee,[3] and Sunghoon Kim[1,4,*]**
[1]National Creative Research Initiatives Center for ARS Network
College of Pharmacy
Seoul National University
Seoul 151-742
[2]Department of Surgery
College of Medicine
Soonchunhyang University
Seoul 140-743
[3]Department of Surgery
College of Medicine
Hanyang University
Seoul 133-791
[4]Genome Research Center
Korea Research Institute of Bioscience and Biotechnology
Daejon
Korea

Summary

p18 was first identified as a factor associated with a macromolecular tRNA synthetase complex. Here we describe the mouse p18 loss-of-function phenotype and a role for p18 in the DNA damage response. Inactivation of both p18 alleles caused embryonic lethality, while heterozygous mice showed high susceptibility to spontaneous tumors. p18 was induced and translocated to the nucleus in response to DNA damage. Expression of p18 resulted in elevated p53 levels, while p18 depletion blocked p53 induction. p18 directly interacted with ATM/ATR in response to DNA damage. The activity of ATM was dependent on the level of p18, suggesting the requirement of p18 for the activation of ATM. Low p18 expression was frequently observed in different human cancer cell lines and tissues. These results suggest that p18 is a haploinsufficient tumor suppressor and a key factor for ATM/ATR-mediated p53 activation.

Introduction

Aminoacyl-tRNA synthetases ligate specific amino acids to their cognate tRNAs in protein synthesis. However, they are functionally versatile proteins involved in various biological processes (Ko et al., 2002). One of the most intriguing characteristics of mammalian tRNA synthetases is that several different aminoacyl-tRNA synthetases form a unique macromolecular protein complex with nonenzyme factors, designated as p43, p38, and p18. Interestingly, many of the components of this complex play unexpected roles in diverse biological processes (Han et al., 2003; Ko et al., 2002). Among the three cofactors in the complex, p18 is the smallest one and shows sequence homology to elongation factor subunits (EF-1) (Quevillon and Mirande, 1996). However, its biological function and significance are not well understood. Here we report that p18 directly interacts with ATM/ATR for the activation of p53 and works as a potent tumor suppressor.

Mammalian ATM and ATR are serine/threonine kinases, which are evolutionarily related to phosphoinositide 3 kinases, and the mutation of ATM is associated with the inheritable chromosomal instability disorder called ataxia telangiectasia (AT) (Savitsky et al., 1995). ATM is a large protein composed of 3056 amino acids, consisting of FAT (FRAP/ATM/TRRAP conserved), PI3K catalytic, and C-terminal domains (Durocher and Jackson, 2001). ATM, ATR, and DNA-dependent protein kinase (DNA-PK) are involved in the DNA repair process and respond to different genotoxic stresses (Yang et al., 2003). Although the functional holoenzyme of DNA-PK consists of the catalytic subunit DNA-PKcs and two Ku subunits, Ku-70 and Ku-80 (Khanna and Jackson, 2001), it is not known whether ATM and ATR require any subunits or cofactors for their activity.

To obtain insight into the physiological significance and working mechanism of p18, we tried to generate p18-depleted mice. However, the loss of p18 resulted in early embryonic lethality. Although this outcome defined p18 as an essential factor for the embryogenesis and viability of the organism, we could not obtain clues to the working mechanism of p18 in vivo. Instead, we found that the p18 heterozygous mice expressed a lower level of p18 as compared to the wild-type littermates, and, as they aged, the heterozygous mice frequently developed various tumors, implying the functional association of p18 with cell cycle control and tumorigenesis. The following molecular and cellular analyses unveiled the activity of p18 as a positive modulator of the ATM response to DNA damage. The functional importance of p18 as tumor suppressor was further supported by examining its expression in human cancer cell lines and tissues.

Results

Spontaneous Tumorigenesis in p18 Heterozygous Mice

The p18 heterozygous mice were generated from embryonic stem cells containing a gene trap insertion at the p18 gene, following the standard protocol of Lexicon Genetics (Zambrowicz et al., 1998). The genotypes of the offspring generated from the intercross between the heterozygous mice were determined by genomic PCR and Southern blot analyses. For the PCR analysis, two primers specific to the p18 gene were designed to generate a 1.5 kb DNA, and one additional primer for the inserted gene trap vector would generate about 0.8 kb DNA with the forward p18 primer. Thus, the wild-type and homozygous mice would produce 1.5 and 0.8 kb

*Correspondence: sungkim@snu.ac.kr

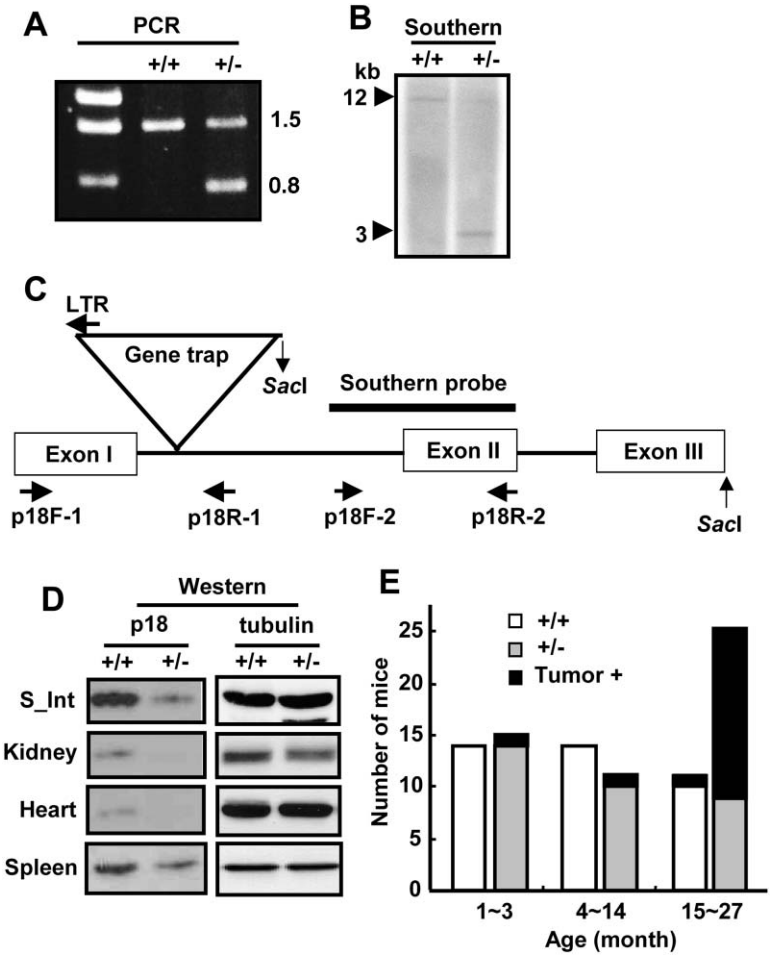

Figure 1. Genetic Characterization and Tumor Occurrence of p18-Deficient Mice

(A) The insertion of the gene trap vector into the p18 gene was determined by a genomic PCR analysis. Genomic DNA was isolated from the mouse tail, and the pair of primers, p18F-1 and p18R-1, was designed to produce a 1.5 kb PCR product from the wild-type DNA. An additional band of 0.8 kb is generated with the primer p18F-1 and LTR binding to the inserted gene trap vector (about 5.7 kb). The data for the homozygous mouse are not available due to embryonic lethality.

(B) Southern blot analysis with SacI-digested genomic DNA, using a DNA probe generated by PCR with the pair of primers p18F-2 and p18R-2. While the wild-type shows one band near 12 kb, the heterozygote generates one additional band of about 3 kb.

(C) Schematic representation of the gene trap insertion into the p18 gene.

(D) Expression of p18 in different $p18^{+/+}$ and $p18^{+/-}$ tissues, as determined by Western blotting with an anti-p18 antibody. Tubulin was used for a loading control.

(E) The mice were classified into three groups according to their ages and the number of mice examined, and the tumor incidence in each group is represented as a bar graph. White and gray bars indicate the total numbers of autopsied wild-type and heterozygous mice, respectively, and the black section in each bar represents the number of mice with tumors.

bands, respectively. Interestingly, all of the examined offspring were determined to be the wild-type or heterozygote generating both the 1.5 and 0.8 kb DNA fragments (Figure 1A). In addition, a Southern blot analysis was performed using the genomic DNAs digested with SacI, with a probe covering the exon II region of p18. While the wild-type DNA showed the hybridization band at about 12 kb, the heterozygous mice generated an additional band at about 3 kb (Figure 1B). In both tests, we could not find offspring with the p18 homozygous genotype (see Supplemental Table S1 at http://www.cell.com/cgi/content/120/2/209/DC1/). The sequencing analysis determined the site of the gene trap vector insertion between exons I and II (Figure 1C). To determine whether the loss of p18 leads to embryonic lethality, we checked the genotypes of embryos on different days after fertilization. Among the total of 83 embryos isolated from 7.5 to 9.5 days, we detected only one embryo on E8.5 containing the homozygous genotype (Supplemental Table S1), indicating that $p18^{-/-}$ mice would be early embryonic lethal. The heterozygous mice were born at a ratio similar to the wild-type littermates (Supplemental Table S1), indicating that about 50% of the heterozygous mice die during the prenatal stage. We then isolated various organs from the $p18^{+/-}$ mice and compared their p18 levels with those of their wild-type littermates by Western blotting with an anti-p18 antibody. In most of the tested organs, the p18 level was significantly lower in the heterozygotes, although the degree of reduction varied depending on the tissue (Figure 1D). The $p18^{+/-}$ mice showed a similar and even slightly higher growth rate as compared to both genders of their wild-type littermates (Supplemental Figure S1). Although the growth and overall morphology of the $p18^{+/-}$ mice looked normal, they spontaneously developed different types of tumors, and the incidence significantly increased when they were older than 15 months (Figure 1E).

Histological Characterization of Tumors

The tumors developed in the $p18^{+/-}$ mice were characterized by H&E staining and immunohistochemistry when necessary. Adenocarcinomas in breast tissue were found in 15- and 23-month-old heterozygous mice (see Supplemental Figure S2A on the *Cell* web site and data not shown), a sarcoma of unknown origin developed in a 22-month-old mouse (Supplemental Figure S2B), and an adenocarcinoma in the seminal vesicle was detected in a 19-month-old mouse (Supplemental Figure S2C). All of these cancers showed typical malignant phenotypes such as anaplasia and invasiveness. Remarkably, the seminal vesicles of the heterozygous mice showed three cystic change cases, one hyperplasia (data not shown), and one adenoma (Supplemental

Figure S2D). Well-differentiated adenocarcinomas originating from the bronchiole epithelium were observed in 17- and 22-month-old mice (Supplemental Figures S2E and S2F). Hepatocarcinoma was detected in a 22-month old mouse (Supplemental Figure S2G). Interestingly, 14 of the 18 tumor-bearing mice developed lymphoma (Supplemental Table S1), originating from the spleen or lymph nodes (Supplemental Figures S2H, S2I, and S2K). Some of the lymphomas metastasized to other organs, such as the liver, kidney, lung, and salivary glands (Supplemental Figures S2J and S2K and data not shown). To confirm this, we performed an immunohistochemical analysis with the anti-B220 monoclonal antibody and differentially diagnosed the lymphoma from reactive hyperplasia, because the white pulp architectures were disrupted by $B220^{+}$ lymphoma cells (Supplemental Figures S2J and S2K). We also found five cases of multiple cancers (Supplemental Table S1). The fact that these tumors spontaneously formed in the heterozygous mice led us to suspect that p18 might be a strong tumor suppressor involved in a general tumorigenic pathway, although it showed more significant linkage to the occurrence of lymphoma.

p18 Regulates the Cell Cycle and Apoptosis

Since a rapid cell cycle and resistance to apoptosis are typical indications for tumorigenesis (Evan and Vousden, 2001), we addressed whether p18 could play a role in cell cycle control. We first compared the cell growth of splenocytes and thymocytes isolated from the wild-type and $p18^{+/-}$ littermates by cell counting. The cells isolated from the $p18^{+/-}$ mice grew faster than did those of the wild-type (Figure 2A). The enhanced proliferation was also observed in the $p18^{+/-}$ MEF cells by tritium-labeled thymidine incorporation (Supplemental Figure S3A). Increased numbers of proliferative cells were detected in various $p18^{+/-}$ tissues by in situ immunofluorescence staining with the proliferation marker Ki-67 (Supplemental Figure S3B). When we measured the cell cycle progression by flow cytometry, the $p18^{+/-}$ splenocytes showed a faster cell cycle than the wild-type cells (Figure 2B).

To obtain insight into the function of p18 during the cell cycle, we synchronized the cell cycle by serum starvation and refeeding and measured the expression level of p18 during different cell cycle phases by Western blotting. p18 was significantly induced during the DNA synthesis phase (Figure 2C). Consistently with the Western blotting, a FACS analysis also showed an increase in the p18 level during S phase (Supplemental Figure S3C). To understand the functional reason for the p18 induction during S phase, we investigated the cellular localization of p18 under growth arrest and proliferating conditions. When the cell growth was suppressed by serum starvation, p18 was mainly located in the cytoplasm. However, it was detected in the nucleus when the cells resumed growth (Figure 2D). The localization of p18 was further examined in different cell cycle stages using tubulin as reference. The nuclear translocation of p18 was clearly observed in the S phase cells (Figure 2E). When the cell cycle was synchronized by double thymidine block, p18 was also nuclear translocated within 1 hr after the cell cycle restarted, and p18 continued to reside in the nuclei during S phase (Supplemental Figure S3D). All of these results indicate that p18 is not only induced but also translocated into the nucleus to exert its activity during DNA synthesis.

We then investigated the role of p18 in the cellular response to stress-induced apoptosis and growth arrest. The $p18^{+/+}$ and $p18^{+/-}$ splenocytes were compared in their response to proapoptotic stress induced by adriamycin, which causes DNA damage. While the number of apoptotic cells significantly increased when the wild-type cells were treated with adriamycin, the $p18^{+/-}$ cells showed resistance to adriamycin-induced apoptosis, as determined by FACS analysis using annexin V and PI staining (Figure 2F and Supplemental Figures S4A and S4B). When the $p18^{+/+}$ and $p18^{+/-}$ cells were treated with adriamycin, the growth of the $p18^{+/-}$ cells was only slightly affected by the adriamycin treatment, while the wild-type cell growth was arrested (Supplemental Figure S4C). We then checked whether the level of p18 was affected by adriamycin treatment. p18 was strongly induced in response to adriamycin, as determined by RT-PCR and Western blot analyses (Figure 2G). The induction of p18 was also observed with other DNA damaging agents, such as UV, actinomycin D (Act. D), and cisplatin (CDPP) (Supplemental Figure S4D). Time course analyses showed that the induction of p18 was achieved within 5–10 min after the exposure to UV or adriamycin (Figure 2H). The nuclear localization of p18, as a consequence of DNA damage, was also observed using U2OS cells (Supplemental Figure S4E). In this cell line, the nuclear foci formed by p18 cells were clearly observed. All of these results suggest that p18 may be involved in a response to DNA damage that may occur during the cell cycle or by genotoxic stresses.

p18 Upregulates p53

Since the tumor suppressor protein p53 plays a major role in the regulation of DNA damage-induced cell cycle arrest and apoptosis (Levine, 1997; Vousden, 2000), we explored the possibility of a functional connection between p18 and p53. Interestingly, the level of p53 was lower in the $p18^{+/-}$ MEFs than that in the wild-type cells, while the ectopic expression of p18 elevated the p53 expression (Figure 3A). To determine whether an increase in p18 would enhance the p53-dependent transcription, we measured the p18-dependent transcription of p21, which is a known target gene of p53. The synthesis of the p21 transcript was enhanced by the ectopic expression of p18, as determined by RT-PCR (Figure 3B). The effect of p18 on the p21 transcription was also checked by a luciferase assay, using a construct bearing p21 promoter fused to the luciferase gene. The luciferase activity was elevated by the transfection of p18 in a dose-dependent manner (Figure 3C), further supporting the significance of p18 for the control of p53 activity. Since the reduction of the p18 level increased the cell proliferation (Figures 2A and 2B and Supplemental Figures S3A and S3B), we tested whether the forced expression of p18 would suppress cell proliferation. As expected, transfection of p18 reduced the proliferation of HCT116 cells, and its antiproliferative activity was abolished in the absence of functional p53 or p21 (Figure 3D), implying that p18 suppresses cell proliferation via p53.

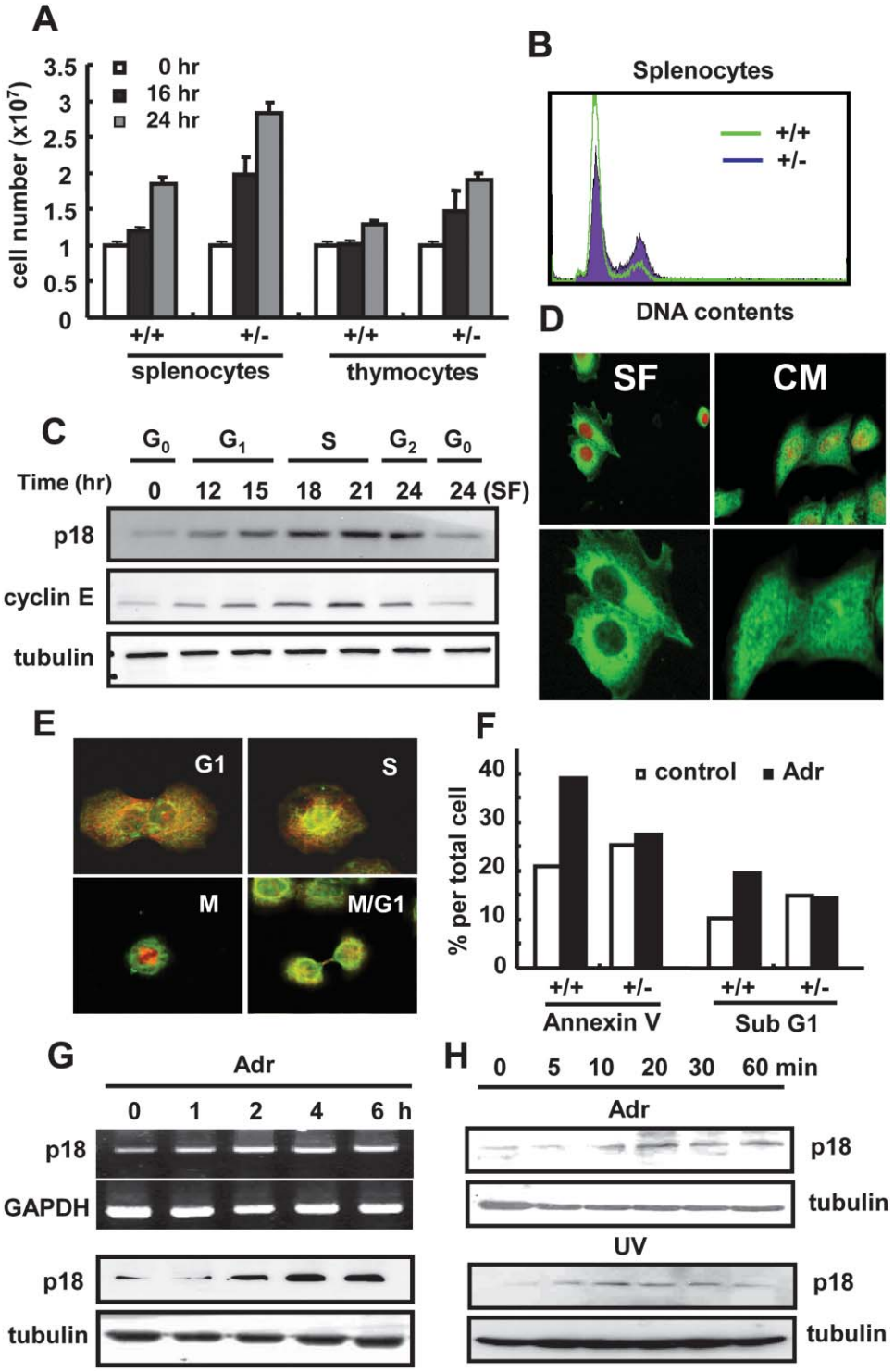

Figure 2. Induction of p18 by DNA Replication and Damage

(A) The cell proliferation rate was measured by cell counting of splenocytes and thymocytes isolated from 4-week-old $p18^{+/+}$ and $p18^{+/-}$ littermates.

(B) Cell cycle progression was determined by flow cytometry. The $p18^{+/+}$ and $p18^{+/-}$ splenocytes were stained with PI after cultivation for 1 day and fixed with 1% PFA. The green line and blue-filled graph indicate $p18^{+/+}$ and $p18^{+/-}$ cells, respectively. For each sample, 20,000 cells were analyzed.

(C) The expression profile of p18 at different cell phases was determined by Western blotting with an anti-p18 antibody. HCT116 cells were starved in serum-free medium for 24 hr, and then complete medium was added to start the cell cycle. The cells were harvested at the indicated times and analyzed for expression of p18. Cyclin E and tubulin were used as markers for the cell cycle and the loading amount, respectively. SF indicates serum-free condition.

To determine whether p18 is critical for p53 activation, we conducted antisense (As) and small interfering (si) RNA techniques to block the expression of p18 and monitored the effect of p18 suppression on the induction of p53. As- or si-p18 reduced the expression of p18, as determined by RT-PCR (Figure 3E). Since As-p18 appeared to be more effective than si-p18 in blocking the expression of p18, we used As-p18 to suppress p18 and evaluated the significance of p18 in p53 induction. A treatment with UV increased the p53 level, whereas the suppression of p18 by As-p18 blocked the induction of p53 (Figure 3F), demonstrating the requirement of p18 for the increase in p53. The transcription of the immediate early p53 target gene, PUMA (Nakano and Vousden, 2001; Yu et al., 2001), was also increased by UV exposure, but the induction was blocked when p18 was suppressed by As-p18 (Figure 3G). All of these results support the idea that p18 is critical for the DNA damage-dependent induction of p53.

Critical Role of ATM in p18-Dependent Regulation of p53

To address how p18 regulates p53, we tested whether p18 directly interacts with p53 by coimmunoprecipitation but could not obtain supportive evidence (data not shown). We then checked the involvement of ATM/ATR, because they are the immediate upstream activators of p53 in response to DNA damage (Canman et al., 1998). To explore the functional involvement of these kinases in the role of p18, we compared the antiproliferative activity of p18 in the isogenic ATM-deficient fibroblasts (AT22IJE-T), harboring the empty vector (S7) and the functional ATM (YZ-5). While p18 suppressed the proliferation of ATM-positive YZ-5 cells, its suppressive effect was not observed in ATM-negative S7 cells (Figure 4A). Apoptosis was also induced by the forced expression of p18, but its proapoptotic activity was also blocked in the absence of functional ATM (Figure 4B).

We also compared the effect of p18 on the induction and activity of p53, using the two isogenic ATM-positive and -negative cell lines used above. Western blotting of p53 showed that it is increased by the transfection of p18 in YZ-5 (ATM-positive) but not in S7 (ATM-negative) cells (Figure 4C). When the activity of p53 was monitored by the expression of its target gene, PUMA, the stimulatory effect of p18 was shown only in YZ-5 cells (Figure 4D). The p18-dependent induction of p53 was blocked by the expression of the kinase-dead domain of ATM (KD-ATM), which inhibits the activity of ATM (Canman et al., 1998), but not by the wild-type ATM (Figure 4E). All of these results support the requirement of ATM for the p18-dependent induction of p53.

p18 Directly Interacts with ATM/ATR in Response to DNA Damage

The results above suggest that p18 somehow activates ATM in response to DNA damage. To elucidate the working mechanism of p18, we performed coimmunoprecipitations of ATM with p18. The cells were incubated under serum-free conditions, and growth was resumed by feeding complete medium. The interaction of ATM with p18 was weak under the growth arrest conditions (serum-free) but became stronger when the cells were treated with adriamycin or fed with the complete medium (Supplemental Figure S5A), suggesting that the interaction between ATM and p18 would be induced by DNA damage that may occur during genotoxic stress or cell growth. The interaction between these two proteins in response to UV and adriamycin increased within 10 min after the introduction of stresses (Figure 5A). However, the dissociation of p18 appeared to be much slower in the adriamycin-treated cells, possibly because the adriamycin was present in the medium throughout the cultivation, while the UV stress would affect the cells only temporarily. Since ATM is an upstream regulator of p53, the interaction between p18 and ATM should be achieved in a p53-independent manner. To test this possibility, we repeated the coimmunoprecipitation experiments in human prostate cancer DU145 cells, which lack functional p53 (Isaacs et al., 1991). p18 bound to ATM in DU145 cells in response to UV and adriamycin treatments (Supplemental Figure S5B), confirming that the interaction of p18 and ATM can take place independently of p53. We then monitored the time course for the nuclear localization of p18 induced by these stresses. In both cases, p18 was translocated into the nucleus within 10 min after the onset of the stress (Figure 5B), consistent with its interaction with ATM.

Next, we tested whether p18 can also interact with ATR. The Flag-tagged ATR was expressed in 293 cells and immunoprecipitated with anti-Flag antibody, and the coprecipitation of p18 was determined by Western blot analysis. The interaction of p18 with ATR was also observed, and it was enhanced by UV irradiation (Figure 5C). The direct interaction of ATM/ATR with p18, and their binding domains, were determined by in vitro pull-down assay. The ATM/ATR homology FAT and PI3K catalytic domains were synthesized in vitro in the presence of [^{35}S] methionine, and each of them was incubated with GST-p18 or GST-p38, and the bound domains were determined by autoradiography. Among the three tested domains, only the FAT domains of ATM and ATR were copurified with GST-p18, but none of these domains bound to GST-p38 (Figure 5D), indicating the direct interaction of p18 with the FAT domains of ATM and ATR despite their limited homology.

(D) The cellular localization of p18 was observed by immunofluorescence microscopy in DU145 cells cultivated in serum-free medium (SF, left column). The cells were fed with complete medium (CM) to resume proliferation and stained as above. The nuclei were stained with PI (red). The cellular localization of p18 (upper) is enlarged to demonstrate that nuclear p18 is present as foci (lower).

(E) The localization of p18 was monitored in DU145 cells at different stages. p18 and tubulin are shown in green and red colors, respectively.

(F) Apoptotic response of splenocytes to adriamycin treatment. The responses of the $p18^{+/+}$ and $p18^{+/-}$ cells to apoptotic stress were compared by monitoring annexin V or PI staining using flow cytometry (see Supplemental Figures S4A and S4B).

(G) Induction of p18 in response to the treatment with adriamycin. The expression of p18 was monitored by RT-PCR (upper) and Western blotting (lower) in HCT116.

(H) Time course for the induction of p18 by UV irradiation and adriamycin treatment, as determined by Western blotting.

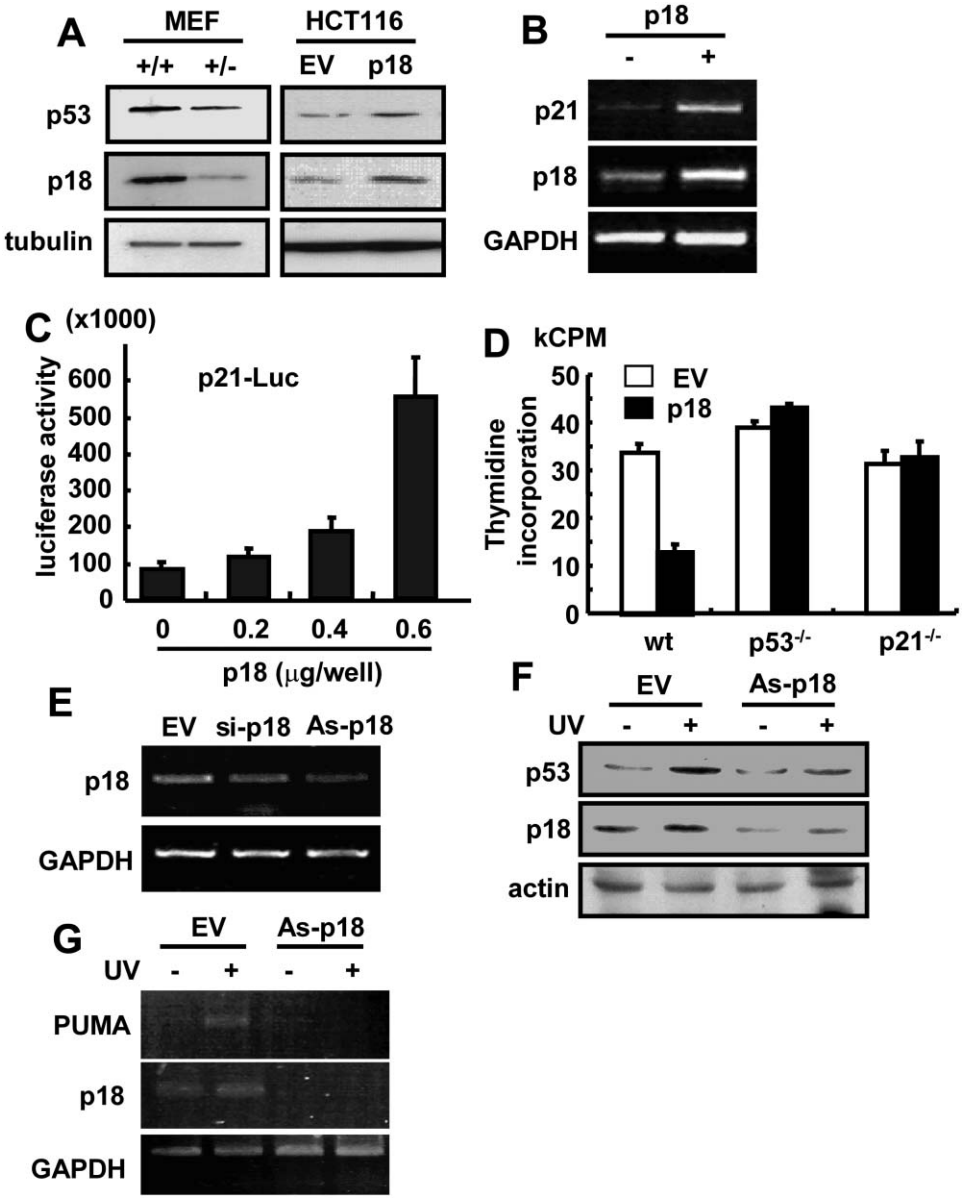

Figure 3. p18 Is Required for p53 Induction

(A) The expression levels of p18 and p53 were compared between $p18^{+/+}$ and $p18^{+/-}$ MEFs (left). The effect of ectopic overexpression of p18 on the level of p53 was performed in HCT116 cells (right). EV stands for empty vector.

(B) The effect of p18 on the p53-dependent transcription of p21 was determined by RT-PCR. HCT116 cells were transfected with p18 (1 μg/ml) and cultivated for 24 hr. The cells were lysed to isolate the RNA, as described in Experimental Procedures, and the synthesis of the p21 transcript was determined by RT-PCR.

(C) The activity of p18 in the p53-dependent transcription of p21 was also determined by a luciferase assay using the construct with the luciferase gene under p21 promoter control. HCT116 cells were transfected with the indicated concentrations of the p18 plasmid and cultivated for 24 hr. The luciferase activity was measured with a luminometer. The β-galactosidase expression vector was also transfected for background calibration.

(D) We transfected the p18 expression vector or EV (2 μg/ml) into HCT116 (wt) and those cells lacking p53 or p21 and checked the effect of p18 on cell proliferation by measuring [^{3}H] thymidine incorporation.

(E) Comparison of the antisense (As) and siRNA on the expression of p18 by RT-PCR. HCT116 cells were transfected with si- or As-p18 (2 μg/ml each) and cultivated for 24 hr.

(F) The significance of p18 on the induction of p53 by UV irradiation (50 J/m^2) was assayed using antisense p18 (As). HCT116 cells, transfected with EV or AS-p18 (2 μg/ml), were subjected to Western blotting for p53 and p18 1 hr after UV exposure. Actin was used for a loading control.

(G) The effect of p18 on the expression of PUMA, an immediate early response gene of p53, was assayed by RT-PCR under the same conditions as above.

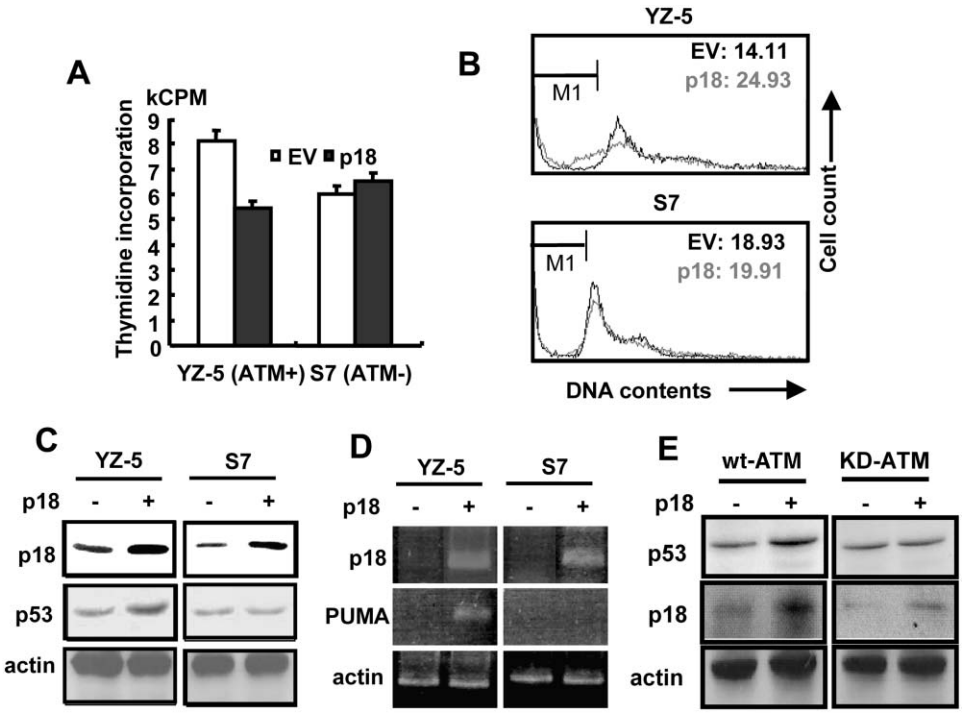

Figure 4. ATM Is Required for p18-Dependent Induction of p53

(A) The requirement of ATM for the antiproliferative activity of p18 was tested in the ATM-deficient human fibroblast line AT22IJE-T carrying the empty vector (S7) or the plasmid encoding functional ATM (YZ-5) (Li et al., 2000). p18 was transfected into these cells, and its effect on cell proliferation was determined by thymidine incorporation.

(B) The significance of ATM in the proapoptotic activity of p18 was also assessed using the two cell lines above. Apoptosis was measured by the portion (%) of sub-G1 cells after PI staining (number above the bar).

(C) The effect of the ectopic expression of p18 on the induction of p53 was determined by Western blotting in the ATM-positive YZ-5 and ATM-negative S7 cells.

(D) Under the same experimental conditions, we assessed the expression of the p53 target gene PUMA by RT-PCR in YZ-5 and S7 cells.

(E) The effect of kinase-dead ATM (KD-ATM) was examined on the p18-dependent induction of p53. HCT116 cells were transfected with p18 in combination with wild-type (wt) or KD-ATM, and the expression levels of p18 and p53 were determined by Western blotting.

p18 Activates ATM

To see whether the activity of ATM is enhanced by its association with p18, we monitored the activity of ATM in a few different ways. We first examined the effect of p18 on the phosphorylation of ATM itself, which indicates its activation. The ectopic expression of p18 increased the phosphorylation of ATM (Figure 6A). While the phosphorylation of ATM was enhanced by adriamycin treatment, it was inhibited by the expression of antisense p18 (As-p18) in HCT116 cells (Figure 6B). The adriamycin-dependent activation of ATM was also blocked in the $p18^{+/-}$ thymocytes (Figure 6C). We also investigated the adriamycin-dependent nuclear foci formation of ATM in the $p18^{+/+}$ and $p18^{+/-}$ cells. The nuclear foci of ATM were observed in the normal cells when they were treated with adriamycin but not in the $p18^{+/-}$ cells (Figure 6D). All of the above results consistently suggest that p18 is required for the activation of ATM.

Low Expression of p18 in Human Cancer Cells and Tissues

To determine whether a functional association of p18 exists with human cancers, we first checked the p18 levels in different human cancer cell lines by RT-PCR. Among the tested cell lines, the expression level of p18 was reduced in HCT116, A549, and H460 cells, although the degree of suppression varied depending on the cell type (Figure 7A). When we compared the expression level of p18 by Western blotting among different lung cancer cell lines, we also observed the results consistent with those obtained by RT-PCR (Figure 7B). These findings suggest that the p18 expression level is reduced in some cancer cell lines. Interestingly, the p18 expression level appears to be linked to the functionality of p53. Namely, the p18 level is low in the cells containing active p53, while it is normal in the cells lacking functional p53 (Figure 7A). Moreover, Raji cells, which display partial p53 activity (Bhatia et al., 1993), appeared to express p18 at an intermediate level between p53-positive and -negative cells. This observation implies that one aberration, in either p18 or p53, may be sufficient to transform the cells, further supporting the possibility that p18 and p53 work in the same signal pathway. To obtain insight into the possible cause for the low level of p18 in some cancer cell lines, we compared the DNA content for the p18 gene by PCR, using isolated genomic DNA as the template. Among the three tested cell lines with low p18 expression, H460 and A549 cells appeared to contain lower amounts of DNA encoding p18 than other cells

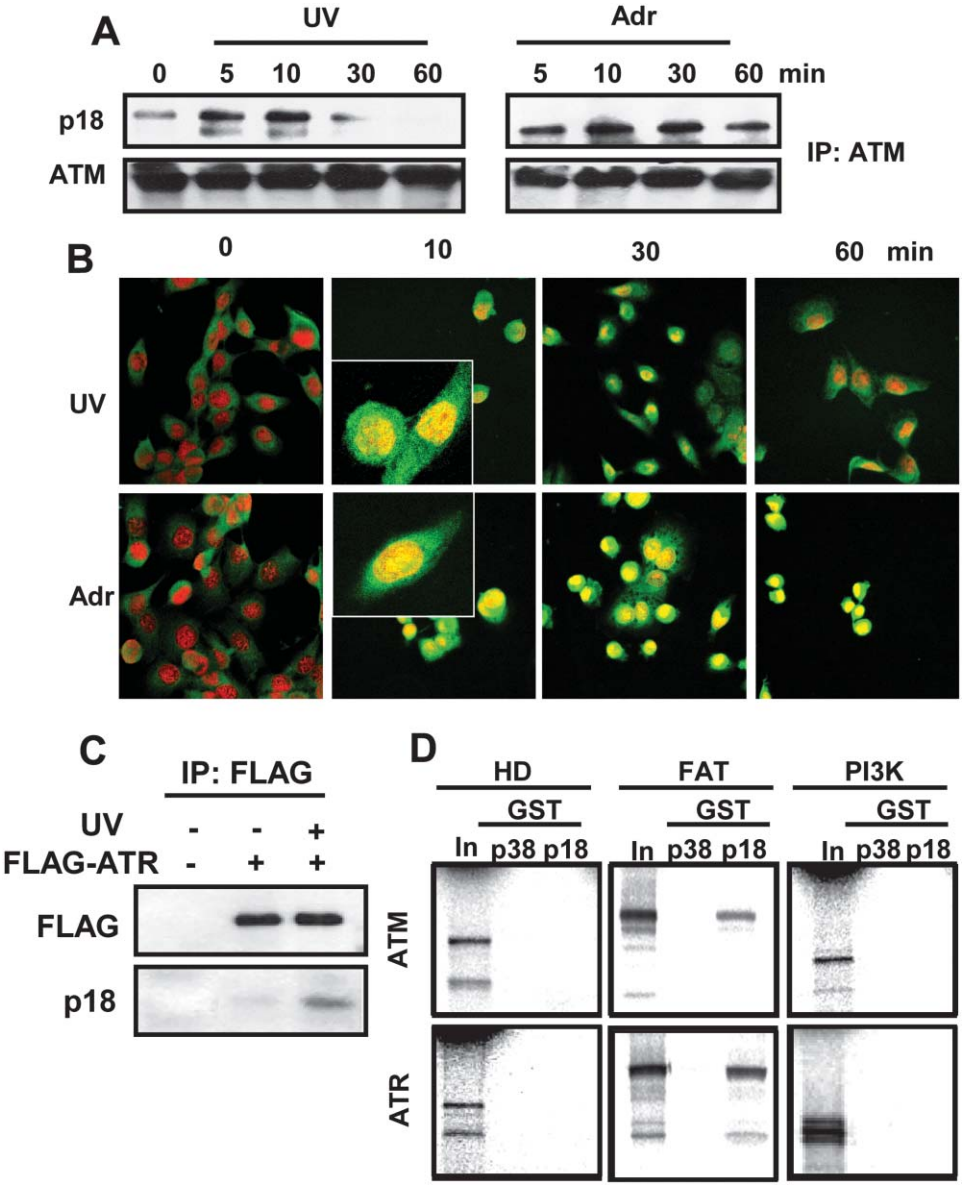

Figure 5. p18 Directly Interacts with ATM

(A) The stress-induced interaction of p18 with ATM was determined by coimmunoprecipitation. HCT116 cells were either UV irradiated or treated with adriamycin (0.4 μg/ml). The cells were harvested at the indicated times and subjected to immunoprecipitation with an anti-ATM antibody, and coimmunoprecipitation of p18 was determined with its specific antibody.

(B) Cellular localization of p18 was determined by immunofluorescence staining in DU145 cells irradiated by UV or treated with adriamycin. p18 and nuclei were stained with the FITC-conjugated secondary antibody and PI, respectively. Insets showed the nuclear as well as the cytoplasmic presence of p18 at 10 min after genotoxic stresses at higher magnification.

(C) The interaction of p18 with ATR was determined by coimmunoprecipitation. 293 cells were transfected with the Flag-tagged ATR, UV irradiated, and immunoprecipitated with the anti-Flag antibody, and coprecipitation of p18 was determined by Western blotting with an anti-p18 antibody.

(D) The domain of ATM/ATR responsible for the interaction (Abraham, 2001) with p18 was determined by in vitro pull-down assay. p18 and p38 (used as a control) were expressed as the GST fusion proteins. The ATM/ATR homology domain (496 aa from 1489 to 1984 in ATM and 459 aa from 1181 to 1639 in ATR), FAT domain (641 aa from 1942 to 2582 in ATM and 698 aa from 1625 to 2322 in ATR), and PI3K catalytic domain (473 aa from 2561 to 3033 in ATM and 403 aa from 2213 to 2615 in ATR) were radioactively synthesized by in vitro translation and reacted with each of GST-18 and -p38 immobilized to glutathione-Sepharose beads. The domains bound to each of the GST fusion proteins were separated by SDS gel electrophoresis and determined by autoradiography. "In" stands for the input of the in vitro-translated domains of ATM and ATR.

(Figure 7C), implying that these cell lines may have lost one p18 allele. In fact, the A549 cell line is already known to have lost one allele of the chromosome region containing the p18 gene (6p24), based on cytogenetic analysis of ATCC.

We then examined the expression of p18 in tissues

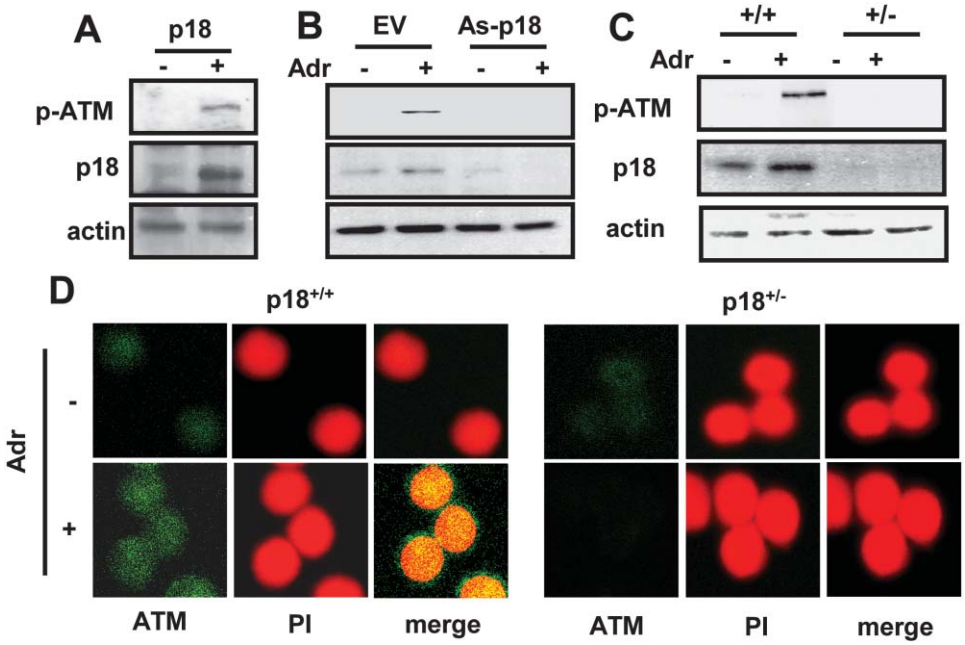

Figure 6. p18-Dependent Activation of ATM

(A) The effect of the ectopic expression of p18 on the phosphorylation of ATM was determined in HCT116 by Western blotting with the antiphosphoserine antibody of ATM (Bakkenist and Kastan, 2003).

(B) The adriamycin-dependent phosphorylation of ATM was compared in the absence and presence of antisense p18 (As-p18) in HCT116.

(C) The adriamycin-dependent activation of ATM was determined in the $p18^{+/+}$ and $p18^{+/-}$ thymocytes by Western blotting.

(D) The effect of p18 on the adriamycin-dependent nuclear foci formation of ATM was compared in the $p18^{+/+}$ and $p18^{+/-}$ splenocytes (×600).

isolated from human cancer patients. Among nine different cases of leukemia (five acute promyelocytic leukemia cases and four chronic myelocytic leukemia cases), low p18 levels were observed in three cases (Figure 7D, patients 1, 5, and 6). In these three cases, the expression of the p53 target gene p21 was also strongly suppressed, corroborating the functional significance of p18 in the regulation of p53. Solid tumors were also found in $p18^{+/-}$ mice, although the frequency was much lower. Therefore, we also compared the p18 level in cancerous tissue with that in normal tissue isolated from human liver cancer patients. From the analyses of 25 different patient samples, we observed the cancer-specific reduction of p18 in 12 cases (Figure 7E and data not shown). All of these results suggest that low p18 expression may be frequently associated with various human cancers.

Discussion

Three different lines of evidence obtained in this work unveiled the activity of p18 as an upstream regulator of p53 via ATM/ATR and as a tumor suppressor. First, the p18 heterozygous mice with the reduced level of p18 show a high incidence of spontaneous tumorigenesis. Second, p18 directly binds and activates ATM to upregulate p53 in response to DNA damage. Third, low p18 expression is observed in human cancer cell lines and tissues. p18 is known to bind to the multi-tRNA synthetase complex with two other auxiliary factors, p43 and p38. Among them, p38 was previously shown to be a critical scaffold for the assembly of the multi-tRNA synthetase complex (Kim et al., 2002). Interestingly, p38 plays an important role in the downregulation of c-*myc* and lung cell differentiation (Kim et al., 2003). Thus, both p18 and p38 are involved in cell cycle control and possibly in tumorigenesis, although their working mechanisms are different. Perhaps they were evolved to coordinate the basal protein synthesis process with important signal pathways for the cell cycle. It would be interesting to see whether a related activity also exists in p43, although it is already known to have complex cytokine activity (Ko et al., 2001; Park et al., 2002).

The loss of p18 resulted in early embryonic lethality, indicating its functional importance in vivo (Supplemental Table S1). Similarly, the genetic eradication of proteins such as Rad51, Chk1/2, and ATR, which are involved in the DNA damage response and repair system, caused early embryonic lethality (de Klein et al., 2000; Lim and Hasty, 1996; Takai et al., 2000). In addition, the $p18^{+/-}$ mice frequently developed lymphoma (Supplemental Figure S2 and Supplemental Table S1), which is consistent with previous reports that the loss of a DNA repair function can evoke lymphoma (Bassing et al., 2003; Celeste et al., 2003). Moreover, p18 is induced and translocated to the nucleus during the DNA synthesis phase and in response to DNA damage (Figures 2D, 2E, and 5B, and Supplemental Figures S3D and S4E) and shows antiproliferative activity like other DNA repair proteins (Figures 3D, 4A, and 4B) (Falck et al., 2001; Lim et al., 2000). All of these phenotypic characteristics and molecular behaviors strongly suggest the role of p18 in the process of DNA repair during DNA replication and stress.

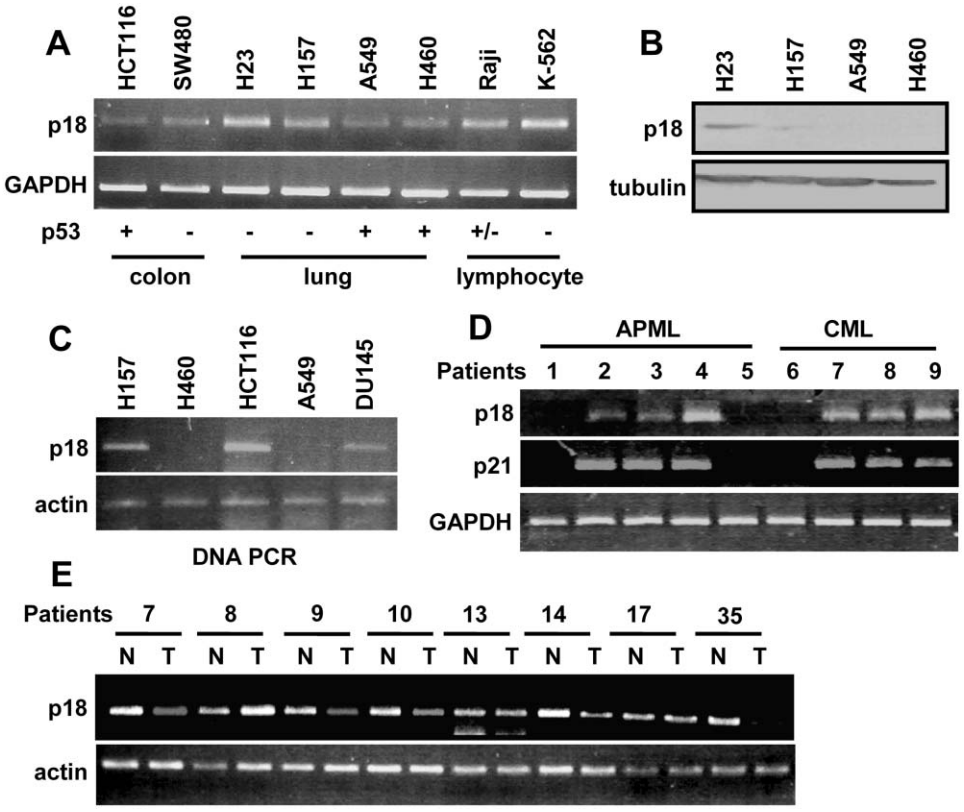

Figure 7. Expression of p18 in Human Cancer Cell Lines and Patient Tissues

(A) The expression level of p18 was examined by RT-PCR in different human cancer cell lines. The functionality of p53 is indicated as + and − in each cell line. Raji cells, which are heterozygous for p53 (Bhatia et al., 1993), are marked as +/−.

(B) The expression of p18 was also checked at the protein level by focusing on lung cancer cell lines.

(C) The DNA contents for the p18 gene in different cancer cell lines were compared by genomic PCR. Actin was used for a loading control. The extended PCR cycle generates the p18 gene product from H460 and A549 cell lines but still to amounts less than those from other cell lines (data not shown).

(D) The expression level of p18 in human leukemia. We obtained total RNAs, isolated from the white blood cells of nine leukemia patients (five APML cases and four CML cases, kindly provided by T.H. Han), and subjected them to RT-PCR to compare the p18 expression levels. The expression of p21 was also measured by RT-PCR.

(E) The p18 expression status in the normal and cancerous regions isolated from human liver cancer patients. Total RNAs were isolated from the normal and cancer regions in the patients' livers, and RT-PCR was conducted to compare the p18 expression levels. Among the 25 informative samples, the results of eight cases are shown. The low expression of p18 was also observed at a similar frequency in other samples (data not shown).

Interestingly, the adriamycin-induced phosphorylation and nuclear foci formation of ATM were severely crippled in the $p18^{+/-}$ cells despite the fact that these cells should still retain one allele of p18 (Figures 6C and 6D). This null-like phenotype may result from the possibility that the heterozygous cells may not have enough p18 to respond to DNA damage. In fact, the p18 level was more severely reduced in most of the different $p18^{+/-}$ cells, even if the heterozygous cells still retained one allele (Figure 1D). p18 showed rapid response to genotoxic stresses (Figures 2H, 5A, and 5B), implying that it would be controlled at the protein level as well as at the transcription level. Indeed, the p18 level was elevated by the inhibition of proteasome activity, and the DNA damage-dependent phosphorylation of p18 was observed (data not shown). Although we have not yet determined the role of the phosphorylation of p18, it is reminiscent of p53, in which turnover is controlled by phosphorylation (Prives, 1998). Thus, p18 appears to be regulated at multiple levels. In this context, it is interesting to note that the ectopic expression of kinase-dead ATM suppressed the basal expression of p18 (Figure 4E), implying another direction of the controlling mechanism. Interestingly, the p18 promoter region appears to harbor a potential binding site for E2F-1(data not shown) that is induced in response to DNA damage via ATM (Lin et al., 2001). Thus, one can expect the regulatory feedback loop between p18 and ATM. In fact, p18 expression was shown to be suppressed in the absence of ATM (Edgar et al., 2002). This regulatory circuit warrants further investigation.

We showed that p18-mediated p53 activation is achieved through a direct interaction with the FAT domain of ATM and ATR (Figure 5D). These proteins contain a PI3 kinase-related catalytic domain flanked by FAT and C-terminal domains. Although the FAT domain itself is not expected to have the catalytic activity, it is thought to play a role in the regulation of the kinase

activity through an intramolecular interaction with the C-terminal region (Bosotti et al., 2000). Perhaps the binding of p18 to the FAT domain may induce a conformational change of ATM/ATR to the active form, although further molecular and biochemical analyses are necessary to understand the details behind p18 activation of ATM. ATM not only participates in cell cycle control via p53 but also is involved in the DNA repair process (Abraham, 2001). If p18 is a general activator of ATM/ATR, it is expected to control DNA repair via these kinases. In fact, we observed a slight enhancement of DNA synthesis when p18 expression was increased by ectopic transfection into p53- or p21-negative cells (Figure 3D). This increase may have resulted from unscheduled DNA synthesis caused by the activated ATM.

p53 is a haploinsufficient tumor suppressor (French et al., 2001; Ide et al., 2003), which exerts multiple activities in the control of cell proliferation and death. Since p18 controls the activity of p53 via ATM, it is expected to suppress tumorigenesis as well. Here we showed that the loss of one p18 allele significantly promoted tumorigenesis (Figure 1E), and low p18 expression is frequently found in different human cancer cell lines and patient tissues (Figure 7). Interestingly, the reduced expression of p18 showed reverse correlation with the functionality of p53 in cancer cell lines (Figure 7A). When we analyzed the functionality of p53 in the cancer cells developed in the $p18^{+/+}$ and $p18^{+/-}$ mice, p53 in the $p18^{+/-}$ cancer cells behaved normally, although p53 did not respond to DNA damage, implying that p53 itself is functional except for its sensitivity to DNA damage due to the defect in the regulatory signal from the p18-ATM line (data not shown). All of these observations, in conjunction with its working mechanism revealed here, further support the notion that p18 should be a critical regulator of p53 and can induce tumorigenesis independently of p53. Comparisons of DNA content demonstrated that some cancer cell lines might have lost one allele of the p18 gene (Figure 7C). In fact, the gene encoding p18 is located in the chromosome region 6p24–25, which was previously shown to be the loss-of-heterozygosity (LOH) region in lymphoma (Baumgartner et al., 2003; Wang et al., 2001). Thus, LOH in this chromosomal region may be responsible for the lower expression of p18, although more vigorous studies are needed to confirm this possibility. Taken together, we conclude that p18 is a haploinsufficient tumor suppressor working in the signal pathway including ATM/ATR and p53 and propose that it could be a useful marker for various cancers and a target for anticancer drug development.

Experimental Procedures

Genetic Disruption of p18 in Mice

To generate p18-deficient mice, we used the gene trap method (Zambrowicz et al., 1998). Within the embryonic stem cell library of the 129/SvEvBrd mouse, in which the gene trap vector was randomly introduced (OmniBank Library, Lexicon Genetics), we identified the OST377244 clone containing the mutated p18 gene. Using this clone, C57BL6 mice heterozygous for p18 were generated following the protocol of Lexicon Genetics. The heterozygous mice were interbred to generate the homozygous offspring. To confirm the insertion of the gene trap vector and its effect on the expression of p18, we performed Southern blot and genomic PCR analyses. For the PCR analysis, genomic DNA was isolated from the mouse tail and subjected to a PCR reaction with a combination of three primers (p18F-1, GCCGGACTTCCTGCTCAATCAAGGTCCTA; p18R-1, CTAGC GGGTGGATAAGTAGTAGTTTCCTCATG; and LTR, CGTTACTTAAG CTAGCTTGCCACCTAC). For Southern blotting, the isolated genomic DNA was digested with SacI, separated by gel electrophoresis, and hybridized with the radioactively labeled 1.5 kb PCR product of the p18 gene prepared with the specific primer (p18F-2, 5′-CAT GAGGAAACTACTACTTATCCACCCGCTAG; p18R-2, 5′-CCTTCAG CAGAGTCTGGGTGTCTTCTTTACTG). The expression of p18 was determined by Western blotting of proteins extracted from 14.5 day mouse embryonic fibroblasts with the polyclonal rabbit anti-p18 antibody.

DNA Construction and Transfection

The cDNAs encoding ATM, ATR, and ATM-KD were kindly provided by M. Kastan (St. Jude Children's Hospital) and S. Elledge (Harvard Medical School). The cDNAs encoding the FAT and C-terminal domains of ATM were obtained by PCR with their specific primers. The primers for the FAT and C-terminal domains were designed to generate cDNAs encoding aa 1970–2582 and aa 2919–3054, respectively. The amplified cDNAs were subcloned into pcDNA3.1/V5-His-TOPO vector for in vitro transcription and translation. To generate the antisense p18 construct, we amplified the N-terminal 200 bp of the p18 gene containing ATG and cloned it into pcDNA3.1 with the reverse orientation. To make the small interfering p18 construct, the IMG-700 (pSuppressorNeo, Imgenex) vector was used for the construction of 21 bp head-to-head hairpins of human p18 (GenBank accession number AB011079). Three 21 bp oligonucleotide sequences specific for human p18 were tested for the suppression of p18 expression. For each construct, two complementary oligonucleotides containing the human p18 sequence were synthesized and annealed to generate double-stranded DNAs, which were cloned into the SalI and XbaI cloning sites of the pSuppressorNeo plasmid according to the manufacturer's recommendations. The most successful sequence found was the 21 bp sequence residing 84 bases 3′ of the ATG, which was site specific to human p18 and lacked significant similarity to other genes. Each of the constructs was introduced to the cells with Geneporter (Gene Therapy Systems) following the manufacturer's protocol.

Flow Cytometry

The cultivated cells were treated or transfected with the indicated drug or vector, fixed with 2% paraformaldehyde for 1 hr at 4°C, washed with ice-cold PBS, and permeabilized with 0.1% Triton X-100 and 0.1% BSA containing PBS. After two washes with ice-cold PBS, the cells were incubated with anti-p18 (1 μg/ml) for 1 hr with agitation at 4°C and with the secondary antibody (anti-mouse-FITC or anti-rabbit FITC; 1 μg/ml) for 45 min in the dark. After washing with PBS, the cells were stained with PI (50 μg/ml) for 20 min and subjected to FACS Calibur (Beckton-Dickinson). For each sample, 15,000 cells were analyzed using the Cell Quest Pro software.

Histological Analyses of Cancers in $p18^{+/-}$ Mice

After sacrificing the mice, the cancer tissues were isolated and fixed with 10% formalin, embedded in paraffin, and subjected to H&E staining. Immunohistochemical staining for the surface marker B220 was performed with a paraffin slide to determine B cell metastasis. After the paraffin was removed with xylene, the slides were incubated with the B220 antibody in blocking buffer (1:100, 5% BSA, and 0.1% Tween 20 in PBS) for 2 hr. After washing with PBS, the tissues were incubated with an avidin-conjugated secondary antibody and the DAB solution.

Luciferase Assay

HCT116 cells were transfected with the vector DNA containing p21-luciferase, in which the luciferase is expressed under p21 promoter control (kindly provided by H.W. Lee, Sungkyunkwan University, Korea) along with the p18 DNA. After lysis, the cell extracts were incubated with the luciferase substrate for 30 min at RT. Then, a 5 μl aliquot of each sample was transferred into the luminometer plate, and the luciferase activity was measured following the manufacturer's protocol (Promega).

Cell Proliferation

Twenty-four hours after transfection with the indicated vectors, the cells were incubated with 1 μCi/ml [^{3}H] thymidine. After washing twice with ice-cold PBS, the cells were incubated with 10% TCA for 0.5 hr at 4°C to precipitate the nucleic acids. After lysis with 0.1 N NaOH, the incorporated radioactive thymidine in the precipitates was quantified by a liquid scintillation counter. The experiments were repeated three times, and the data were averaged.

Cell Cycle Control

To synchronize the cell cycle, we treated the cells with 2 mM thymidine (Sigma) for 16 hr and transferred the cells into thymidine-free medium for 12 hr. The cells were then incubated with thymidine-containing medium for 16 hr. The medium was then removed, and the cells were incubated in thymidine-free medium and harvested at the indicated times.

RT-PCR

After cell lysis with Sol. D solution (4 M guanidine thiocyanate, 1% laurosarcosine, 25 mM sodium citrate, and 0.1% β-mercaptoenthanol), the cell extracts were incubated with acidic phenol and chloroform containing 4% isoamylalcohol. After vortexing, the mixtures were centrifuged at 14,000 rpm. We collected the upper layer and added isopropanol for RNA precipitation. After washing with 100% ethanol, 1 μg of RNA dissolved in distilled water was used as the template for RT-PCR with the sets of specific primers. Information about the primers and PCR conditions will be provided upon request.

Western Blotting and Coimmunoprecipitation

Cells were dissolved in RIPA buffer containing a protease inhibitor cocktail, and the lysates were centrifuged at 14,000 rpm for 30 min. We then fractionated 20 μg of the extracted proteins by SDS-PAGE. To examine the interaction between p18 and ATM/ATR, the protein extracts were incubated with normal IgG and protein A/G agarose for 2 hr and then centrifuged to remove nonspecific IgG binding proteins. After centrifugation, we collected the supernatant and added the antibody against ATM or FLAG (2 μg/sample). After an incubation for 2 hr at 4°C with agitation, we added protein A/G agarose. After washing twice with ice-cold PBS and once with RIPA, the precipitates were dissolved in SDS sample buffer and separated by SDS-PAGE. To detect ATM, we used a 6% SDS-PAGE gel. After the proteins were transferred to a PVDF membrane, the coimmunoprecipitation of p18 was determined with an anti-p18 monoclonal antibody and a horseradish peroxidase-conjugated secondary antibody. The monoclonal antibody for total p53 (DO-1) and polyclonal rabbit antibody for p53 phosphorylated at Ser15 were purchased from Santa Cruz and Cell Signaling, respectively. The phosphoserine (Ser1981)-ATM-specific antibody was obtained from Rockland.

In Vitro Pull-Down

p18 and p38 (used as a control) were expressed as GST fusion proteins and immobilized to glutathione-Sepharose 4B (Pharmacia). The cDNA fragments encoding the ATM/ATR homology domain, FAT domain, and PI3K domain were obtained by PCR from human ATM and ATR using their specific primers and cloned into pcDNA3.1/V5-His-TOPO vector for in vitro transcription and translation (Promega). Aliquots (10 μl) of TNT products were incubated with 5 μg of GST-p18 or GST-p38 immobilized on the beads in 100 μl of PBS containing 0.5% Triton X-100, 0.5 mM EDTA, and 0.5 mM phenylmethylsulfonyl fluoride. The beads were vigorously washed with the binding buffer, and the bound proteins were eluted, resolved by SDS-PAGE, and determined by autoradiography.

Immunostaining

Cells were fixed with 100% methanol for 10 min at −20°C and then incubated with blocking buffer (0.1% BSA and 0.05% Triton X-100 containing PBS) for 1 hr at RT. After washing with ice-cold PBS, the cells were incubated with the anti-p18 antibody diluted in blocking buffer and then reacted with a FITC- or PE-conjugated secondary antibody. After mounting, the cellular localization of p18 was observed with an immunofluorescent confocal microscope (Bio-Rad μ-Radiance).

Apoptosis

In situ apoptosis detection was conducted with an Apoptag fluorescein kit (Oncor) following the manufacturer's manual. Apoptotic cells were visualized by confocal microscopy. We also measured apoptosis using the splenocytes isolated from the p18 wild-type and heterozygous littermates. The cells were incubated with FITC-conjugated annexin V or propidium iodide for 5 min. After a brief wash with PBS, the cells were subjected to FACS analysis with the FL-1H detector.

Acknowledgments

We thank Tae Hee Han for providing the RNAs isolated from leukemia patients; Dae Sik Lim, Michael B. Kastan, Stephen J. Elledge, Yosef Shiloh, and Han Woong Lee for materials; and Kenji Kamino for consultations regarding the tumor analyses in mice. This work was supported by a grant from National Creative Research Initiatives of the Ministry of Science and Technology, Korea.

Received: March 19, 2004
Revised: September 7, 2004
Accepted: November 22, 2004
Published: January 27, 2005

References

Abraham, R.T. (2001). Cell cycle checkpoint signaling through the ATM and ATR kinases. Genes Dev. *15*, 2177–2196.

Bakkenist, C.J., and Kastan, M.B. (2003). DNA damage activates ATM through intermolecular autophosphorylation and dimer dissociation. Nature *421*, 499–506.

Bassing, C.H., Suh, H., Ferguson, D.O., Chua, K.F., Manis, J., Eckersdorff, M., Gleason, M., Bronson, R., Lee, C., and Alt, F.W. (2003). Histone H2AX: a dosage-dependent suppressor of oncogenic translocations and tumors. Cell *114*, 359–370.

Baumgartner, A.K., Zettl, A., Chott, A., Ott, G., Muller-Hermelink, H.K., and Starostik, P. (2003). High frequency of genetic aberrations in enteropathy-type T-cell lymphoma. Lab. Invest. *83*, 1509–1516.

Bhatia, K., Goldschmidts, W., Gutierrez, M., Gaidano, G., Dalla-Favera, R., and Magrath, I. (1993). Hemi- or homozygosity: a requirement for some but not other p53 mutant proteins to accumulate and exert a pathogenetic effect. FASEB J. *7*, 951–956.

Bosotti, R., Isacchi, A., and Sonnhammer, E.L. (2000). FAT: a novel domain in PIK-related kinases. Trends Biochem. Sci. *25*, 225–227.

Canman, C.E., Lim, D.S., Cimprich, K.A., Taya, Y., Tamai, K., Sakaguchi, K., Appella, E., Kastan, M.B., and Siliciano, J.D. (1998). Activation of the ATM kinase by ionizing radiation and phosphorylation of p53. Science *281*, 1677–1679.

Celeste, A., Difilippantonio, S., Difilippantonio, M.J., Fernandez-Capetillo, O., Pilch, D.R., Sedelnikova, O.A., Eckhaus, M., Ried, T., Bonner, W.M., and Nussenzweig, A. (2003). H2AX haploinsufficiency modifies genomic stability and tumor susceptibility. Cell *114*, 371–383.

de Klein, A., Muijtjens, M., van Os, R., Verhoeven, Y., Smit, B., Carr, A.M., Lehmann, A.R., and Hoeijmakers, J.H. (2000). Targeted disruption of the cell-cycle checkpoint gene ATR leads to early embryonic lethality in mice. Curr. Biol. *10*, 479–482.

Durocher, D., and Jackson, S.P. (2001). DNA-PK, ATM and ATR as sensors of DNA damage: variations on a theme? Curr. Opin. Cell Biol. *13*, 225–231.

Edgar, R., Domrachev, M., and Lash, A.E. (2002). Gene Expression Omnibus: NCBI gene expression and hybridization array data repository. Nucleic Acids Res. *30*, 207–210.

Evan, G.I., and Vousden, K.H. (2001). Proliferation, cell cycle and apoptosis in cancer. Nature *411*, 342–348.

Falck, J., Mailand, N., Syljuasen, R.G., Bartek, J., and Lukas, J. (2001). The ATM-Chk2-Cdc25A checkpoint pathway guards against radioresistant DNA synthesis. Nature *410*, 842–847.

French, J.E., Lacks, G.D., Trempus, C., Dunnick, J.K., Foley, J., Mahler, J., Tice, R.R., and Tennant, R.W. (2001). Loss of heterozygosity frequency at the Trp53 locus in p53-deficient (+/−) mouse

tumors is carcinogen-and tissue-dependent. Carcinogenesis *22*, 99–106.

Han, J.M., Kim, J.Y., and Kim, S. (2003). Molecular network and functional implications of macromolecular tRNA synthetase complex. Biochem. Biophys. Res. Commun. *303*, 985–993.

Ide, F., Kitada, M., Sakashita, H., Kusama, K., Tanaka, K., and Ishikawa, T. (2003). p53 haploinsufficiency profoundly accelerates the onset of tongue tumors in mice lacking the xeroderma pigmentosum group A gene. Am. J. Pathol. *163*, 1729–1733.

Isaacs, W.B., Carter, B.S., and Ewing, C.M. (1991). Wild-type p53 suppresses growth of human prostate cancer cells containing mutant p53 alleles. Cancer Res. *51*, 4716–4720.

Khanna, K.K., and Jackson, S.P. (2001). DNA double-strand breaks: signaling, repair and the cancer connection. Nat. Genet. *27*, 247–254.

Kim, J.Y., Kang, Y.S., Lee, J.W., Kim, H.J., Ahn, Y.H., Park, H., Ko, Y.G., and Kim, S. (2002). p38 is essential for the assembly and stability of macromolecular tRNA synthetase complex: implications for its physiological significance. Proc. Natl. Acad. Sci. USA *99*, 7912–7916.

Kim, M.J., Park, B.-J., Kang, Y.-S., Kim, H.J., Park, J.-H., Kang, J.W., Lee, S.W., Han, J.M., Lee, H.-W., and Kim, S. (2003). Downregulation of fuse-binding protein and c-myc by tRNA synthetase cofactor, p38, is required for lung differentiation. Nat. Genet. *34*, 330–336.

Ko, Y.-G., Park, H., Kim, T., Lee, J.-W., Park, S.G., Seol, W., Kim, J.E., Lee, W.-H., Kim, S.-H., Park, J.E., and Kim, S. (2001). A cofactor of tRNA synthetase, p43, is secreted to up-regulate proinflammatory genes. J. Biol. Chem. *276*, 23028–23033.

Ko, Y.G., Park, H., and Kim, S. (2002). Novel regulatory interactions and activities of mammalian tRNA synthetases. Proteomics *2*, 1304–1310.

Levine, A.J. (1997). p53, the cellular gatekeeper for growth and division. Cell *88*, 323–331.

Li, S., Ting, N.S., Zheng, L., Chen, P.L., Ziv, Y., Shiloh, Y., Lee, E.Y., and Lee, W.H. (2000). Functional link of BRCA1 and ataxia telangiectasia gene product in DNA damage response. Nature *406*, 210–215.

Lim, D.S., and Hasty, P. (1996). A mutation in mouse rad51 results in an early embryonic lethal that is suppressed by a mutation in p53. Mol. Cell. Biol. *16*, 7133–7143.

Lim, D.S., Kim, S.T., Xu, B., Maser, R.S., Lin, J., Petrini, J.H., and Kastan, M.B. (2000). ATM phosphorylates p95/nbs1 in an S-phase checkpoint pathway. Nature *404*, 613–617.

Lin, W.C., Lin, F.T., and Nevins, J.R. (2001). Selective induction of E2F1 in response to DNA damage, mediated by ATM-dependent phosphorylation. Genes Dev. *15*, 1833–1844.

Nakano, K., and Vousden, K.H. (2001). PUMA, a novel proapoptotic gene, is induced by p53. Mol. Cell *7*, 683–694.

Park, S.G., Kang, Y.S., Ahn, Y.H., Lee, S.H., Kim, K.R., Kim, K.W., Koh, G.Y., Ko, Y.G., and Kim, S. (2002). Dose-dependent biphasic activity of tRNA synthetase-associating factor, p43, in angiogenesis. J. Biol. Chem. *277*, 45243–45248.

Prives, C. (1998). Signaling to p53: breaking the MDM2-p53 circuit. Cell *95*, 5–8.

Quevillon, S., and Mirande, M. (1996). The p18 component of the multisynthetase complex shares a protein motif with the beta and gamma subunits of eukaryotic elongation factor 1. FEBS Lett. *395*, 63–67.

Savitsky, K., Sfez, S., Tagle, D.A., Ziv, Y., Sartiel, A., Collins, F.S., Shiloh, Y., and Rotman, G. (1995). The complete sequence of the coding region of the ATM gene reveals similarity to cell cycle regulators in different species. Hum. Mol. Genet. *4*, 2025–2032.

Takai, H., Tominaga, K., Motoyama, N., Minamishima, Y.A., Nagahama, H., Tsukiyama, T., Ikeda, K., Nakayama, K., and Nakanishi, M. (2000). Aberrant cell cycle checkpoint function and early embryonic death in Chk1(−/−) mice. Genes Dev. *14*, 1439–1447.

Vousden, K.H. (2000). p53: death star. Cell *103*, 691–694.

Wang, V.W., Bell, D.A., Berkowitz, R.S., and Mok, S.C. (2001). Whole genome amplification and high-throughput allelotyping identified five distinct deletion regions on chromosomes 5 and 6 in microdissected early-stage ovarian tumors. Cancer Res. *61*, 4169–4174.

Yang, J., Yu, Y., Hamrick, H.E., and Duerksen-Hughes, P.J. (2003). ATM, ATR and DNA-PK: initiators of the cellular genotoxic stress responses. Carcinogenesis *24*, 1571–1580.

Yu, J., Zhang, L., Hwang, P.M., Kinzler, K.W., and Vogelstein, B. (2001). PUMA induces the rapid apoptosis of colorectal cancer cells. Mol. Cell *7*, 673–682.

Zambrowicz, B.P., Friedrich, G.A., Buxton, E.C., Lilleberg, S.L., Person, C., and Sands, A.T. (1998). Disruption and sequence identification of 2,000 genes in mouse embryonic stem cells. Nature *392*, 608–611.

Accession Numbers

The GenBank accession number for the *human p18* sequence reported in this paper is AB011079.